

A combined experimental and theoretical study on realizing and using laser controlled torsion of molecules

C. B. Madsen* and L. B. Madsen

*Lundbeck Foundation Theoretical Center for Quantum System Research,
Department of Physics and Astronomy, Aarhus University, 8000 Aarhus C, Denmark*

S. S. Viftrup, M. P. Johansson, T. B. Poulsen, L. Holmegaard, V. Kumarappan, and K. A. Jørgensen

Department of Chemistry, Aarhus University, 8000 Aarhus C, Denmark

H. Stapelfeldt†

Department of Chemistry and Interdisciplinary Nanoscience Center (iNANO), Aarhus University, 8000 Aarhus C, Denmark

It is demonstrated that strong laser pulses can introduce torsional motion in the axially chiral molecule 3,5-difluoro-3',5'-dibromo-biphenyl (DFDBrBPh). A nanosecond laser pulse spatially aligns the stereogenic carbon-carbon (C-C) bond axis allowing a perpendicularly polarized, intense femtosecond pulse to initiate torsional motion accompanied by a rotation about the fixed axis. We monitor the induced motion by femtosecond time-resolved Coulomb explosion imaging. Our theoretical analysis corroborates the experimental findings and on the basis of these results we discuss future applications of laser induced torsion, viz., time-resolved studies of de-racemization and laser controlled molecular junctions based on molecules with torsion.

I. INTRODUCTION

Gaining control over the external and the internal degrees of freedom of molecules is of great interest for a range of areas in molecular science. One approach, dating as far back as the 1920s [1, 2], relies on the application of inhomogeneous (static or low frequency) magnetic and electric fields. This has proven most useful for controlling the full three-dimensional motion of molecules, including control of the velocity distribution, bringing molecules to a stand still, storing them for extended periods of times and trapping them in a confined volume (for a recent review see [3]). An alternative and complementary approach relies on the use of non-resonant non-ionizing laser fields typically supplied by pulsed lasers. Many studies during the last decade have shown that strong non-resonant laser fields can effectively manipulate the external degrees of freedom of isolated gas phase molecules. The manipulation results from laser-induced forces and torques due to the interaction between the induced dipole moment and the laser field itself. Examples of manipulation include deflection [4], focusing [5] and slowing [6] of molecules through the dependence of the non-resonant polarizability interaction on the intensity distribution in a laser focus. Likewise, the dependence of the induced dipole interaction on molecular orientation has proven highly useful for controlling the rotation of a variety of molecules [7]. In particular, the spatial orientation of molecules can be sharply confined with respect to axes that are fixed in the laboratory.

Molecular manipulation by induced dipole forces ex-

tends beyond the external degrees of freedom and has also been demonstrated for the internal degrees of freedom such as vibrational motion [8] in molecular hydrogen. Notably, the electrical field from laser pulses can modify energy potential barriers such that photoinduced bond breakage of a small linear molecule is guided to yield a desired final product [9, 10].

In the case of larger molecules control of the lowest frequency vibrational modes attracts special interest since some of these modes correspond to motion along well-defined reaction coordinates separating two conformational minima (conformers). Although many molecules contain large number of conformers it is often just two conformers that dominate important chemical properties, for instance chirality. A particularly important example is found in axially chiral molecules [11, 12] such as biaryl systems. In these molecules rotation about a single stereogenic carbon-carbon (C-C) bond axis changes the molecule from one enantiomer into the opposite enantiomer (mirror image). Recently, we demonstrated that the laser-induced nonresonant polarizability interaction can also be used to influence the internal rotation of an axially chiral molecule around the stereogenic C-C bond axis [13]. In particular, we showed that by fixing the C-C bond axis of a substituted biphenyl molecule in space, using laser induced alignment by a long laser pulse, it was possible to initiate torsional motion of the two phenyl rings by a short laser pulse polarized perpendicular to the fixed axis. The purpose of the present work is to extend our recent paper [13]. In particular, we discuss our theoretical modelling in detail.

*Corresponding author: cbm@phys.au.dk

†Corresponding author: henriks@chem.au.dk

II. OUTLINE OF THE STRATEGY FOR LASER CONTROLLED TORSION

A ns laser pulse aligns [7] the stereogenic axis of 3,5-difluoro-3',5'-dibromo-biphenyl (DFDBrBPh) along its polarization. This enables a much shorter fs pulse, which we will refer to as the kick pulse, to both initiate torsional motion and set the molecule into rotation around the fixed axis. The internal as well as external rotational motion is monitored by fs time-resolved Coulomb explosion imaging.

The inset of Fig. 1 shows a model of the DFDBrBPh molecule with the stereogenic axis marked by red. According to our quantum chemical calculations, the laser-free torsional potential, illustrated by the red dotted curve in Fig. 1, has minima at dihedral angles of $\langle\phi_d\rangle = \pm 39^\circ$ corresponding to the R_a and S_a enantiomeric forms, and where the dihedral angle is the angle between the two phenyl rings. The twisted equilibrium shape is characteristic of biphenyl compounds. The traditional view is that this non-planarity results from competition between stabilization via conjugation of the π -orbital systems and steric repulsion between the ortho-positioned atoms [14]. We might mention that alternative explanations have recently been discussed [15, 16, 17]. Our strategy for controlling ϕ_d relies on a transient modification of the field-free potential curve by a fs kick pulse (Fig. 1). The modification, caused by the nonresonant polarizability interaction [7, 9, 18] converts the initial stationary quantum states, localized near the minima of the torsional potential, into vibrational wave packets, i.e., coherent superpositions of several quantum states. The temporal evolution of these wave packets gives rise to time-dependent torsional motion, and the grey and the black curves in Fig. 1 show the calculated expectation values of ϕ_d for a particular set of laser parameters. The stereogenic C-C bond axis is fixed in the laboratory frame by adiabatic alignment utilizing a moderately intense, linearly polarized ns laser pulse [7, 19]. The ns pulse is intense enough to keep the C-C axis tightly confined, yet weak enough to modify the torsional potential only slightly. The fs kick pulse is applied with its polarization perpendicular to the aligned C-C bond axis to ensure primarily influence on torsion while avoiding other possible vibrational motion.

The DFDBrBPh compound is prepared as a racemate and the experiment is carried out on isolated molecules at rotational temperatures of a few Kelvin. Under these conditions we have equal numbers of molecules initially localized in the -39° or 39° conformation (see Fig. 1) and no thermally induced transitions between the two conformations occur. The intense probe pulse, sent at time t_p with respect to the kick pulse, removes several electrons from the molecules, thereby triggering Coulomb explosion into ionic fragments. In particular, the Br^+ and F^+ fragment ions recoil in the planes defined by the Br- and F-phenyl rings. By recording the velocities of both ion species with two-dimensional ion imaging [19], we determine the instantaneous orientation of each of the

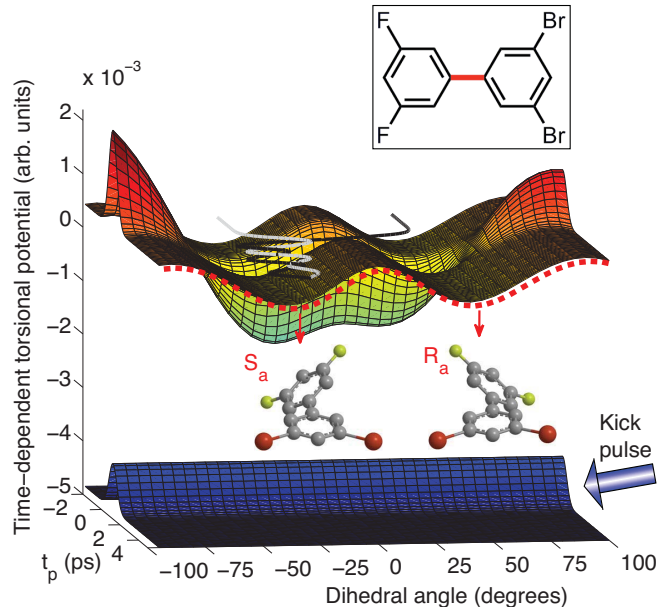


FIG. 1: (Color online) To illustrate the principle of laser-induced torsion and time-resolved de-racemization we show the calculated kick pulse induced time-dependent torsional potential as a function of time measured with respect to the center of the pulse and dihedral angle ϕ_d between the Br- and F-phenyl planes. The asymmetry in the potential is obtained by orienting the molecules (here with the Br-phenyl plane out of the paper), 3D aligning them, and by polarizing the kick pulse at an angle of 13° with respect to the second most polarizable axis (SMPA) (see Fig. 2). The red dotted curve at large times illustrates the laser-free time-independent torsional potential. For the S_a enantiomer, starting out with $\langle\phi_d\rangle_i = -39^\circ$, the time varying potential induces an oscillatory motion (grey curve) corresponding to torsion confined within the initial well. By contrast, due to the induced asymmetry between the two wells, the initial R_a enantiomer is traversing the central torsional barrier, and ends up as an S_a enantiomer undergoing internal rotation (black curve). The kick pulse has an intensity of $1.2 \times 10^{13} \text{ W/cm}^2$ and a duration of 1.0 ps (FWHM). The torsional motion may be monitored by fs time-resolved Coulomb explosion imaging. The inset shows a model of the DFDBrBPh molecule with the stereogenic axis marked by red (grey).

two phenyl planes at the time of the probe pulse.

III. THEORETICAL METHODS

A. Modelling the dynamics of the molecule

To account for the motion of the nuclei of the DFDBrBPh molecule we make use of two sets of coordinate systems (see Fig. 2): A molecular fixed (MF) frame attached to the molecule and a laboratory fixed (LF) frame specified by the lasers. The MF coordinates are chosen

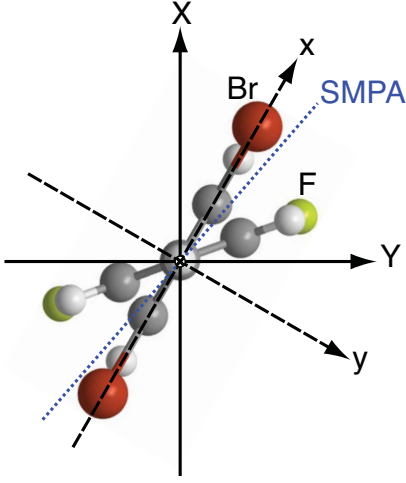


FIG. 2: Model of DFDBrBPh along with the molecular fixed (MF) xyz and the laboratory fixed XYZ coordinate axes. The dotted line indicates the second most polarizable axis (SMPA), which is located 11° from the Br-phenyl ring and 28° from the F-phenyl ring.

with the z axis along the stereogenic axis pointing from the phenyl ring with the bromines towards the phenyl ring with the fluorines, and the x axis is chosen along the phenyl ring with the bromines. The LF coordinates are chosen with the Z axis along the polarization direction of the ns pulse and the X axis along the kick pulse polarization direction. In agreement with the experimental observations (cf. Sec. V), we assume that the stereogenic axis of the DFDBrBPh molecule is aligned along the Z axis. Also, we neglect all normal modes, except the lowest one, which corresponds to torsion (see Sec. IIIB for details on quantum chemical calculations, justifying, e.g., this assumption). In this simplified situation and in the absence of the kick pulse the task is reduced to describing the coupled rotations of the two (rigid) phenyl rings of the molecule as given in the LF frame by the Hamiltonian [Atomic units, $m_e = e = a_0 = \hbar = 1$, are used throughout unless indicated otherwise]

$$H_{\text{mol}} = -\frac{1}{2I_{\text{Br}}} \frac{\partial^2}{\partial \phi_{\text{Br}}^2} - \frac{1}{2I_{\text{F}}} \frac{\partial^2}{\partial \phi_{\text{F}}^2} + V_{\text{tor}}(\phi_{\text{Br}} - \phi_{\text{F}}), \quad (1)$$

where $\phi_i, i = \text{Br}, \text{F}$, is the angle of the i phenyl ring with respect to the kick pulse polarization axis, I_i the moment of inertia for rotation of the i phenyl ring around the stereogenic axis ($I_{\text{Br}} = 8911925$, $I_{\text{F}} = 1864705$) and $V_{\text{tor}}(\phi_{\text{Br}} - \phi_{\text{F}})$ is the laser-free torsional potential as obtained from quantum chemical calculations (Fig. 3). By changing the coordinates to the dihedral angle $\phi_d = \phi_{\text{Br}} - \phi_{\text{F}}$ between the two phenyl rings and the weighted azimuthal angle $\Phi = (1 - \eta)\phi_{\text{Br}} + \eta\phi_{\text{F}}$, characterizing the rotation of the molecule, with $\eta = I_{\text{F}}/(I_{\text{F}} + I_{\text{Br}})$, we

obtain

$$H_{\text{mol}} = \left(-\frac{1}{2I} \frac{\partial^2}{\partial \Phi^2} \right) + \left(-\frac{1}{2I_{\text{rel}}} \frac{\partial^2}{\partial \phi_d^2} + V_{\text{tor}}(\phi_d) \right) = H_{\Phi} + H_{\phi_d}. \quad (2)$$

Here $I = I_{\text{Br}} + I_{\text{F}}$ is the total moment of inertia of the molecule for rotation around the stereogenic axis and $I_{\text{rel}} = I_{\text{Br}}I_{\text{F}}/I$ is a relative moment of inertia for the two phenyl rings around the axis. A full rotation of either phenyl ring leaves us with the same molecule implying 2π -periodic boundary conditions of the eigenfunctions of H_{mol} from Eq. (1), i.e., $\psi(\phi_{\text{Br}} + 2\pi m, \phi_{\text{F}} + 2\pi n) = \psi(\phi_{\text{Br}}, \phi_{\text{F}})$, with m and n integers. We shall assume that this property also applies to Φ and ϕ_d , so that we simply need to consider eigenfunctions $\tilde{\psi}(\Phi, \phi_d) = \xi(\Phi)\chi(\phi_d)$ of Eq. (2) that separates into rotation of the molecule as described by the 2π -periodic function $\xi(\Phi)$ and torsion accounted for by the 2π -periodic function $\chi(\phi_d)$. [Rigorously, the bounds for Φ depend on ϕ_d [20]. At the time scales of interest, however, a molecule generally only makes a small fraction of a full rotation so that the effect of Φ - ϕ_d coupling is negligible.] The separation is physically motivated by considering the energy scales related to rotation and torsion. The energy scale of the prior is given by $\hbar^2/(2I) = 1.3 \mu\text{eV}$. For torsion, on the other hand, the relevant energy is determined by the torsional potential, and a harmonic approximation of the potential near the minimum at 39° yields a frequency corresponding to the energy 3.1 meV. Using that the period of motion is of the order Planck's constant divided by the energy, we therefore see that the molecule rotates (Φ change) on a nanosecond time scale, whereas the torsion (ϕ_d change) is of picosecond duration.

The small energy separation of the rotational levels compared to that of the torsional levels implies that many rotational states will be occupied in thermal equilibrium. Consequently, we expect the Φ dynamics to behave classically (see also Fig. 7), and we only treat the torsional dynamics quantum mechanically. The torsion is described by the stationary Schrödinger equation

$$H_{\phi_d}|\chi_\nu\rangle = E_\nu|\chi_\nu\rangle, \quad (3)$$

with $\nu = 1, 2, \dots$ denoting the energy eigenstates. To solve this equation we expand the Hamiltonian onto an orthonormal basis of 2π -periodic functions, which we diagonalize. The eigenstates below the torsional barriers exhibit an almost exact fourfold degeneracy, and linear combinations of the approximately degenerate states will also be stable at the time scales of the experiment. In particular, we can produce such stable states that are localized in the wells of the torsional potential. We will denote these states by $|L_{\nu_{\text{min}}}^{(i)}\rangle$, with $i = 1, 2, 3, 4$ and ν_{min} the smallest ν of the four degenerate states. In Fig. 3 we show the first four energy eigenstates and the corresponding localized states along with the torsional potential. The experiment is generally carried out on a gas of

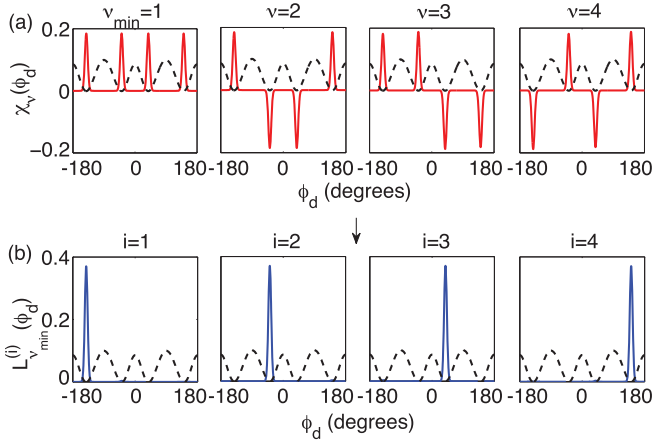


FIG. 3: The field-free torsional states. (a) The four first (almost) degenerate energy eigenstates lying 1.71 meV above the minimum of the torsional potential. From linear combinations of these we obtain the corresponding four localized states shown in (b). The torsional potential is indicated with a dashed line.

molecules in a mixed state given by the density matrix

$$\rho(t_0) = \sum_{\nu_{\min}} \sum_{i=1}^4 P_{\nu_{\min}}^{(i)} |L_{\nu_{\min}}^{(i)}\rangle \langle L_{\nu_{\min}}^{(i)}| + \sum_{\nu} P_{\nu} |\chi_{\nu}\rangle \langle \chi_{\nu}|, \quad (4)$$

with the P 's being weight factors that sum to unity, and where the latter sum includes the states above the torsional barrier. The kick pulse introduces dynamics that we determine from the alignment potential created by the pulse. By definition $\mathbf{F}(t) = F_0(t)\hat{\mathbf{X}}$ for the kick pulse, and we use a Gaussian envelope $F_0(t) = F_0 \exp\{-\ln(2)[t/(\tau_{\text{FWHM}}/2)]^2/2\}$ corresponding to an intensity full width at half maximum (FWHM) of τ_{FWHM} . We calculate the polarizability tensor in the MF frame as a function of the dihedral angle (see Table I) and consequently transform into the LF frame by the application of directional cosine matrices [21]. We then arrive at the interaction

$$\begin{aligned} V_{\text{kick}}(\Phi, \phi_d, t) = & -\frac{1}{4} F_0^2(t) [\alpha_{xx}(\phi_d) \cos^2(\Phi + \eta\phi_d) \\ & + \alpha_{yy}(\phi_d) \sin^2(\Phi + \eta\phi_d) \\ & - 2\alpha_{xy}(\phi_d) \cos(\Phi + \eta\phi_d) \sin(\Phi + \eta\phi_d)]. \end{aligned} \quad (5)$$

For the succeeding analysis it is helpful to note a few qualitative features of the potential and we refer to Fig. 2 for graphical guidance. For a fixed dihedral angle the potential is minimal when the second most polarizable axis (SMPA), which is located 11° from the Br-phenyl ring and 28° from the F-phenyl ring, is parallel to the X axis. We will denote this by the \parallel -geometry. Conversely, the potential is maximal if the molecule is rotated 90° from the \parallel -geometry, and we will denote this by the \perp -geometry. Next, in the \parallel -geometry the potential favors

a reduction of the dihedral angle, whereas an increase of the dihedral angle is resulting from the \perp -geometry. Hence, the overall effect of the kick pulse will be to align the molecules into the \parallel -geometry and drive a change of the dihedral angle.

We proceed with the quantitative analysis of the field-induced dynamics. The state $|\chi_{\nu}\rangle$ is no longer an eigenstate of the torsion when the kick pulse is applied, but will develop into a wave packet

$$|\chi_{\nu}\rangle \rightarrow |\chi_{\nu}^{\Phi}(t)\rangle = \sum_{\nu'} c_{\nu'}^{\Phi}(t) e^{-iE_{\nu'}(t-t_0)} |\chi_{\nu'}\rangle \quad (6)$$

with the coefficients determined by

$$\dot{c}_{\nu'}^{\Phi}(t) = -i \sum_{\nu} c_{\nu}^{\Phi}(t) e^{-i(E_{\nu} - E_{\nu'})(t-t_0)} \langle \chi_{\nu'} | V_{\text{kick}}(\Phi, t) | \chi_{\nu} \rangle. \quad (7)$$

Once we find these new states of torsion the expectation value of any operator O can be evaluated by tracing the product of the density matrix with the operator, i.e., $\langle O(t) \rangle = \text{Tr}[\rho(t)O]$. In particular, we need the expectation value of the dihedral angle and of the kick potential from Eq. (5). From the latter we obtain the torque, which causes the molecule to rotate into the \parallel -geometry. If the molecule lies at an angle Φ it is exposed to a torque $-\partial \langle V_{\text{kick}}(\Phi, t) \rangle / \partial \Phi$ directed along the Z axis and hence achieves an angular acceleration given by

$$I\ddot{\Phi} = -\frac{\partial \langle V_{\text{kick}}(\Phi, t) \rangle}{\partial \Phi}. \quad (8)$$

Along with the initial conditions given at Eq. (4), the Eqs. (7) and (8) provide a set of coupled differential equations that may be integrated to obtain the coordinates $\Phi(t)$ and $\langle \phi_d(t) \rangle$ at time t . Rather than solving these coupled equations, we, however, assume that the angle Φ has the constant value Φ_0 during the short time interval of the kick pulse, and we integrate Eq. (8) twice to arrive at

$$\Phi(t) = \Phi_0 - t \frac{1}{I} \left(\frac{\partial}{\partial \Phi} \int_{-\infty}^{\infty} dt' \langle V_{\text{kick}}(\Phi, t') \rangle \right) \Big|_{\Phi=\Phi_0}. \quad (9)$$

Consistently, we solve Eq. (7) with Φ fixed at Φ_0 .

For the present work we start out with a distribution of values for Φ_0 in the interval $[-\pi, \pi]$ along with an initial density matrix, $\rho(t_0)$ and we propagate each member of the distribution according to Eqs. (7) and (9). This procedure yields an ensemble of $\Phi(t)$'s and $\langle \phi_d(t) \rangle$'s and we finally employ the relations $\phi_{\text{Br}}(t) = \Phi(t) + \eta \langle \phi_d(t) \rangle$ and $\phi_{\text{F}}(t) = \Phi(t) - (1 - \eta) \langle \phi_d(t) \rangle$ to find the angular distributions of bromines and flourines.

B. Quantum chemical calculations

To determine the field-free torsional potential we obtain the geometries of DFDBrBPh in various conformations at the density functional theory level [22, 23], with

TABLE I: The table lists the relevant polarizability components, α_{ij} , of DFDBrBPh in the MF frame as a function of the dihedral angle, ϕ_d . The components are π -periodic and fulfill $\alpha_{xx}(\phi_d) = \alpha_{xx}(\pi - \phi_d)$, $\alpha_{yy}(\phi_d) = \alpha_{yy}(\pi - \phi_d)$ and $\alpha_{xy}(\phi_d) = -\alpha_{xy}(\pi - \phi_d)$. Also, $\alpha_{yx} = \alpha_{xy}$.

ϕ_d	(degrees)	0	15	30	45	60	75	90
α_{xx}	(atomic units)	217.694	215.590	209.463	200.975	192.431	186.240	184.048
α_{yy}	(atomic units)	92.352	95.201	102.634	112.658	122.693	130.015	132.639
α_{xy}	(atomic units)	0.000	-9.488	-16.360	-18.810	-16.225	-9.295	0.000

B3LYP, Becke’s three-parameter hybrid exchange functional [24] in connection with the Lee-Yang-Parr correlation [25] functional. We model the correlation of the uniform electron gas with the Vosko-Wilk-Nusair VWN5 formulation [26], and we use doubly polarized triple-zeta quality basis-sets, TZVPP [27]. This level of theory has been shown to be suitable for the study of biphenyls [28]. To scan the potential energy surface of the relative torsional angle of the phenyl rings we optimize all coordinates except the torsional angle.

We do all electronic structure calculations with the TURBOMOLE 5.10 program suite [29]. In Table I we give the dynamic polarizabilities computed at a laser wavelength of 1064 nm. We note that the polarisabilities are quite stable with respect to choice of laser frequency. Using a value of 800 nm changes the individual components only minutely (maximally by 2%). The differences between static and dynamic polarisabilities are equally small. We calculate the vibrational frequencies analytically [30], and a normal mode analysis, using internal coordinates, shows that the lowest frequency vibration corresponds almost purely to the torsion of the phenyl rings. We compute vibrational Raman cross-sections from derivatives of the polarizability tensor with respect to the normal modes of vibration. Table II shows the frequencies and Raman cross sections of the lowest vibrations of DFDBrBPh, computed at B3LYP/TZVPP level. The results provide the justification for assuming that the kick pulse primarily interacts with the lowest normal mode, since its Raman scattering cross section is over four times higher than the second lowest normal mode and 20 times higher than any other normal mode. We note that the character of the second lowest (and second strongest Raman active) mode contains no torsional motion.

IV. EXPERIMENTAL METHODS

A. Synthesis of 3,5-dibromo-3’,5’-difluorobiphenyl

To a round-bottom flask equipped with a magnetic stirring bar under argon we add 3,5-difluorophenylboronic acid (474 mg, 3.0 mmol), 1,3,5-tribromobenzene (1134 mg, 3.6 mmol), and Pd(PPh₃)₄ (69.6 mg, 2 mol%). The flask is then evacuated and backfilled with argon twice. To this mixture of solids we add toluene (18 mL, degassed), EtOH (6 mL, degassed), and 2M aq.

TABLE II: Vibrational frequencies and relative Raman cross sections of the eight lowest lying normal modes of DFDBrBPh, computed at B3LYP/TZVPP level.

mode	frequency (cm ⁻¹)	cross section (%)
ν_1	23.9	100.0
ν_2	55.7	21.4
ν_3	60.7	2.8
ν_4	111.9	5.1
ν_5	145.2	1.3
ν_6	194.7	3.6
ν_7	195.3	1.3
ν_8	213.4	0.8

Na₂CO₃ (3 mL, degassed). We next heat the mixture to 90°C under argon for 5.5 h and cool it to room temperature. The mixture is diluted with water and extracted three times with Et₂O. We dry the combined organic fractions with MgSO₄, filter and concentrate to give approximately 1.4 g of a crude mixture. Based on NMR we find that this mixture contains both the desired mono-Suzuki coupling product [31], double-coupled products, and a homo-coupling product from the boronic acid. Careful column chromatography on SiO₂ eluting with n-hexane and c-hexane finally allows us to isolate 182 mg 3,5-dibromo-3’,5’-difluorobiphenyl (DFDBrBPh) as a white amorphous solid (contains <3% of the homo-coupling product DFDBrBPh). NMR spectroscopic data (see also Fig. 4): ¹H NMR δ (400 MHz, CDCl₃) 7.69 (t, J 1.7 Hz, 1H), 7.61 (d, J 1.7 Hz, 2H), 7.05 (m, 2H), 6.85 (m, 1H). ¹³C NMR δ (100 MHz, CDCl₃) 163.5 (2C), 142.3, 141.5, 133.8, 128.9 (2C), 123.5 (2C), 110.1 (2C), 103.8. Elemental analysis, calculated: C 41.42%, H 1.74%, Br 45.92%; found: C 41.20%, 1.66%, Br 45.90%.

B. Setup of the laser experiment

A schematic of the experimental setup is shown in Fig. 5. Less than hundred milligram of solid DFDBrBPh is heated to 130°C and expanded in 90 bar of He into vacuum using a pulsed Even-Lavie valve [19, 32]. The resulting supersonic molecular beam is skimmed and subsequently crossed by three, focused, pulsed laser beams at 90°. The first laser beam originates from a Q-switched Nd:YAG laser and consists of 9-ns-long pulses at 1064 nm. It is focused to a spotsize $\omega_0 \sim 35 \mu\text{m}$ yielding a

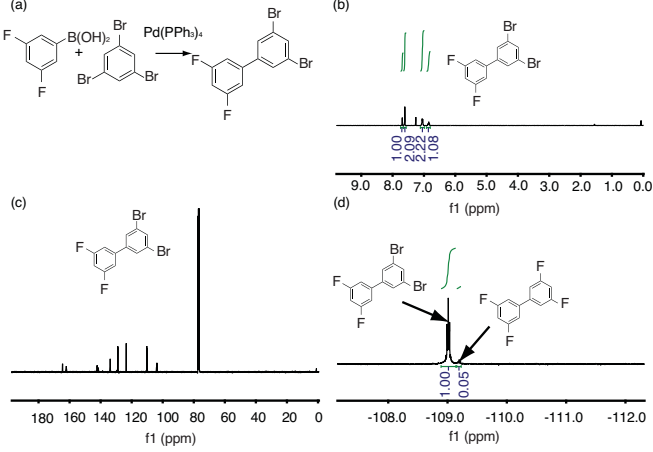


FIG. 4: (Color online) (a), Synthesis of DFDBrBPh by Pd-catalyzed cross-coupling. (b)-(d), NMR-spectra of synthetic DFDBrBPh. Integrated signals are indicated by green (grey) curves, and the corresponding numbers are situated directly below the respective curves.

peak intensity of $\sim 7 \times 10^{11} \text{ W/cm}^2$. The purpose of these pulses is to align the stereogenic axis of the DFDBrBPh molecules. The second laser beam consists of 0.7-ps-long kick pulses ($\lambda = 800 \text{ nm}$), obtained by passing part of the output from an amplified Ti:Sapphire fs laser system through a grating stretcher. The spotsize of $\omega_0 = 43 \mu\text{m}$ yields a peak intensity of $\sim 5 \times 10^{12} \text{ W/cm}^2$. These kick pulses are used to induce torsion and rotation of the molecules. The third laser beam consists of 25-fs-long pulses, which we achieve by passing another part of the output from the Ti:Sapphire system through a hollow wave guide compressor setup. The pulses have a spotsize $\omega_0 = 25 \mu\text{m}$ and a peak intensity of $\sim 2 \times 10^{14} \text{ W/cm}^2$. These probe pulses Coulomb explode the molecules and the produced ions are extracted by a weak static electric field, in a velocity imaging geometry, and projected onto a two-dimensional detector, consisting of a micro channel plate (MCP) detector backed by a phosphor screen. We detect the F^+ and Br^+ ions separately by time gating of the MCP detector around the respective arrival times of the ions. We record the ion images on the phosphor screen by a CCD camera and determine the coordinates of each individual ion hit. Figure 6(a) displays the ion images of F^+ and Br^+ at selected probe times.

V. RESULTS AND DISCUSSION

First, we establish that the ns pulse is able to hold the C-C bond axis of DFDBrBPh along its polarization direction. At $t_p = -0.87 \text{ ps}$ the F^+ image, displayed in Fig. 6(a), is almost circularly symmetric and the small deviation from circular symmetry is explained by noting that the kick pulse has a finite value at -0.87 ps . The

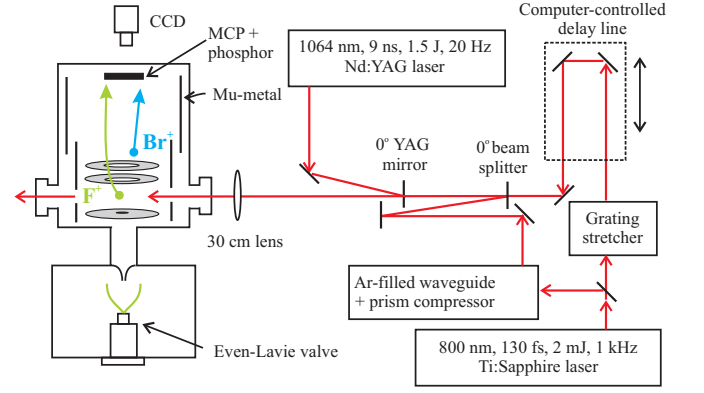


FIG. 5: (Color online) Schematic representation of the experimental setup, showing the vacuum system and the three laser beam paths. The Nd:YAG (alignment) pulses and the probe pulses are polarized vertically, i.e., perpendicular to the detector plane, whereas the fs kick pulse is polarized in the plane of the detector.

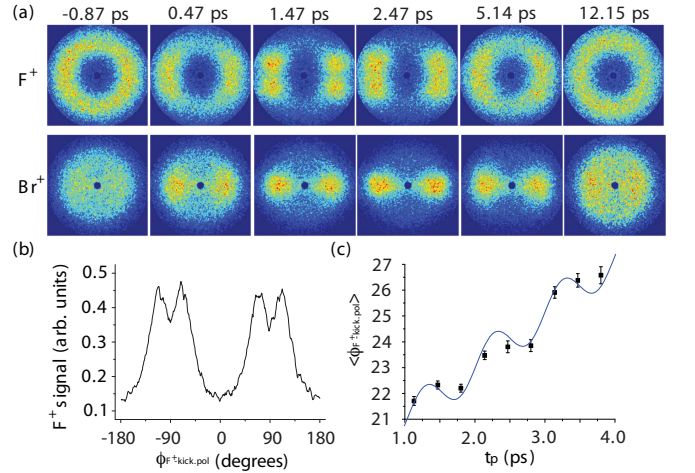


FIG. 6: (Color online) (a) Ion images of F^+ and Br^+ fragments at probe times t_p . The ns pulse is polarized perpendicularly to the image (detector) plane and the $5 \times 10^{12} \text{ W/cm}^2$, 0.7 ps (FWHM) kick pulse is polarized horizontally. (b) Angular distribution of the F^+ ions, at $t_p = 1.47 \text{ ps}$, obtained by radially integrating the corresponding F^+ ion image. The splitting of the pairwise peaks is twice the average angle, $\langle \phi_{\text{F}^+-\text{kick_pol}} \rangle$, between the F^+ ion recoil (and thus the F-phenyl plane) and the kick pulse polarization. (c) $\langle \phi_{\text{F}^+-\text{kick_pol}} \rangle$ as a function of t_p , for times where a clear four-peak structure is visible in the angular distributions. The curve is a fit of the sum of a linear and a harmonic function to the experimental points (squares).

absence of ions in the innermost region is only compatible with the C-C bond axis being aligned perpendicular to the detector plane and the F-phenyl planes uniformly distributed around the C-C bond axis. The corresponding Br^+ image is also essentially circularly symmetric although the hollow-out of the center is not as pronounced as for F^+ .

Next, we investigate the effect of the kick pulse. Already at $t_p = 0.47$ ps the circular symmetry is broken and both F^+ and Br^+ ions start to localize around the polarization direction of the kick pulse. The F^+ ions remain within the radial range of the ring structure, which shows that the kick pulse does not cause any significant distortion of the C-C bond axis alignment but rather initiates an overall rotation of the molecule around this axis. The latter is expected since the torque imparted by the kick pulse will force the SMPA (Fig. 2) to align along the kick pulse polarization after a delay determined by the kick strength. At $t_p = 1.47$ ps the localization sharpens for both ion species, but whereas the Br^+ ions are simply more localized around the polarization axis the F^+ ion distribution exhibits a four dot structure. This behaviour is compatible with alignment of the SMPA along the kick pulse polarization. In the limit of perfect SMPA alignment, the Br^+ ions would appear as two pairs of strongly localized regions on the detector corresponding to molecules with their Br-phenyl plane located either 11° clockwise or counterclockwise to the SMPA. Each pair of Br^+ ions would then be angularly separated by 22° . In practise and consistent with theory (see Fig. 8) the SMPA alignment is not strong enough to resolve the two Br^+ regions. It is, however, sharp enough to resolve the two pairs of F^+ ion hits due to the much larger offset (28°) of the F-phenyl plane from the SMPA. At $t_p = 2.47$ ps the Br^+ distribution has localized further showing that the Br-phenyl plane has rotated into stronger alignment with the kick pulse polarization. If the torsion was unaffected, i.e., ϕ_d remained unchanged, the F^+ ion image at $t_p = 2.47$ ps should exhibit a distinct four-dot structure similar to the image at $t_p = 1.47$ ps but with a larger angular splitting between the ion regions in each of the two pairs. Clearly, the four-dot structure at 2.47 ps is significantly blurred compared to the case at 1.47 ps. Thus, we conclude that the kick pulse not only sets the molecule into controlled rotation around the C-C axis, it also initiates torsional motion.

Beyond 3.8 ps the angular confinement of both the F^+ and the Br^+ ions is gradually lost due to continued rotation around the C-C axis with dihedral dynamics imposed, and the images for both ion species eventually regain their circularly symmetric form (see images at 12.15 ps in Fig. 6(a)) identical to the pre-kick pulse images at -0.87 ps.

Further insight into the effect of the kick pulse is obtained by analyzing the angular distribution of the F^+ ions as a function of t_p . An example of the F^+ angular distribution at $t_p = 1.47$ ps is shown in Fig. 6(b). Figure 6(c) displays the average angle between the F-phenyl rings and the kick pulse polarization as a function of t_p in the time interval where a clear four-peak structure is visible in the angular distributions. The increase from 22.5° at 1.47 ps to 26.5° at 3.8 ps shows that the F-phenyl plane gradually moves away from the kick pulse polarization due to the overall rotation of the molecule around the C-C bond axis, and we ascribe the recurrent

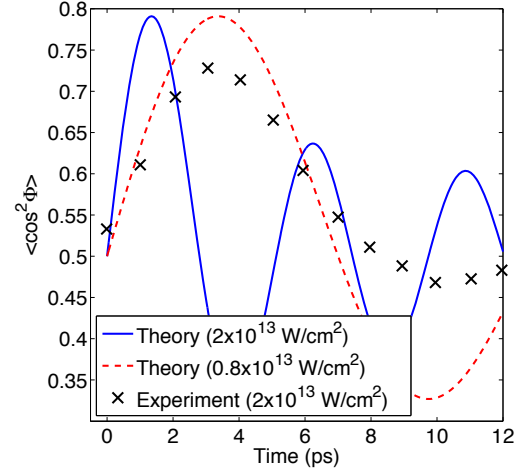


FIG. 7: (Color online) Comparison of the classical model for rotation at various intensities with the experiment of Ref. [33]. The theory captures the laser induced rotation within the first 12 ps, but generally overestimates the degree of angular confinement.

dips to a periodical variation in ϕ_d . We estimate the period to be ~ 1 ps and the amplitude to $\sim 0.6^\circ$ for this oscillation.

Before presenting the theoretical results on DFD-BrBPh, we want to confirm the validity of the classical treatment of rotation. To this end we apply the model to a test case, where the simpler 3,5-difluoriodobenzene (DFIB) has its most polarizable axis fixed by a ns laser pulse and is then set into rotation about this axis by an orthogonally polarized femtosecond pulse. Here, there is no torsion and the rotational dynamics have been observed directly recently [33]. In Fig. 7, we compare the theoretical and experimental results and find good agreement.

Figure 8 shows the results of a calculation with laser parameters identical to the experimental values and an initial rotational temperature of 0 K. Prior to the kick pulse the angular distributions of the Br- and F-phenyl rings are isotropic as in the experiment. Maximum alignment of the SMPA occurs at 1.3 ps and the confinement of the F-phenyl rings at a large angle with respect to the kick pulse polarization (cf. middle panel, Fig. 8(a)) explains the distinct four-dot structure observed at $t_p = 1.47$ ps in the experimental F^+ ion image (Fig. 6(a)). Also, at $t_p = 1.47$ ps the confinement of the Br-phenyl rings at a small angle with respect to the kick pulse polarization predicts a much less distinct, if any, four-dot structure in good agreement with the Br^+ ion image. At $t_p = 2.47$ ps the angular localization of the F-phenyl rings has broadened (right panel, Fig. 8(a)) and a blurred four-dot structure is seen, consistent with the experimental result at $t_p = 2.47$ ps. The distribution of the Br-phenyl rings is also broadened (right panel, Fig. 8(b)), but remains localized around the kick pulse polarization

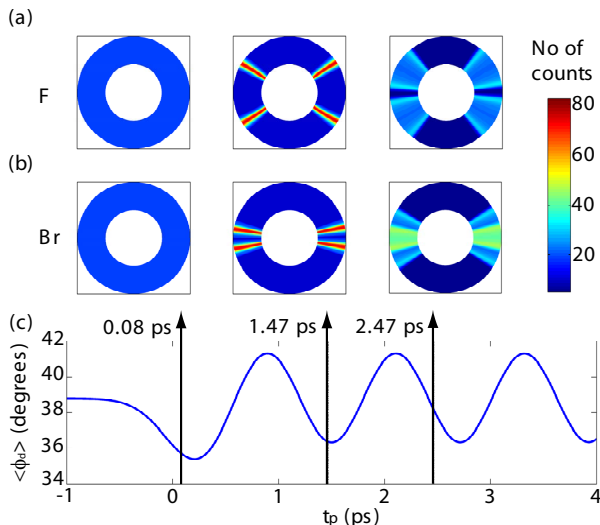


FIG. 8: (Color online) Angular distributions of (a) F-phenyl and (b) Br-phenyl rings at $t_p = 0.08, 1.47$ and 2.47 ps. (c) Expectation value of the dihedral angle for a molecule starting out with the SMPA aligned along the kick pulse polarization. The kick pulse is as in Fig. 6.

fully consistent with the Br^+ ion distribution, recorded at 2.47 ps.

The theoretical value $\langle \phi_d \rangle$ exhibits oscillations (Fig. 8(c)) with a period of ~ 1.2 ps and amplitude of $\sim 2.45^\circ$. The period agrees well with the experimental value (~ 1 ps), and smaller modulation in $\langle \phi_d \rangle$ is expected in the experiment ($\sim 0.6^\circ$) partly since here the SMPA is not pre-aligned and partly due to deviations from the stated laser peak intensity. The behavior is ascribed to a wave packet of normal modes in the torsional double well potential (Fig. 3(b)) for a molecule starting out with the SMPA aligned. The qualitative agreement of Figs. 6(b) and 8(c) corroborates the interpretation of the kick pulse inducing time-dependent torsional motion.

VI. PERSPECTIVES

We will now discuss some perspectives of the demonstrated laser control of torsion. For one thing, we suggest a time-resolved study of de-racemization [34, 35, 36, 37, 38], where one enantiomer is steered into its mirror form. To do this we break the inversion symmetry of the C-C bond axis by orienting each molecule. This allows us to discriminate between the two enantiomeric forms. Theory [39, 40] and experiment [41, 42] show that orientation can be added to 3D alignment by combining the ns alignment pulse with a static electric field. Next, the excitation of torsional motion is optimized by eliminating initial rotation around the C-C bond through alignment of the SMPA (Fig. 2) prior to the kick pulse using an elliptically rather than a linearly polarized ns pulse [7, 43]. Finally, the interaction strength between the molecule

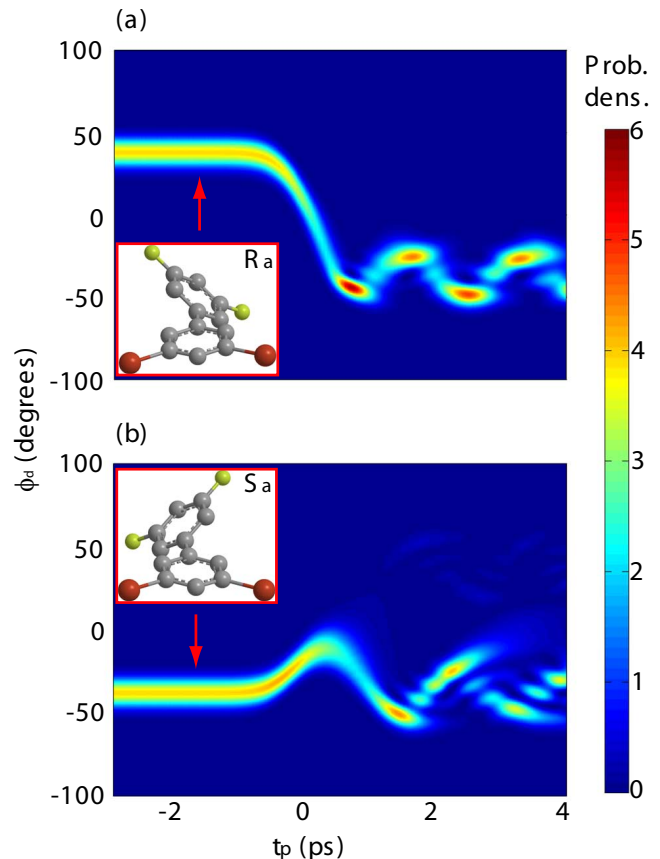


FIG. 9: (Color online) Time evolution of the dihedral angle for a molecule starting out as (a) an R_a or (b) an S_a enantiomer. Initially, the molecule is 3D oriented with the Br-phenyl end pointing out of the paper and the SMPA aligned at an angle of 13° with respect to the kick pulse polarization. The kick pulse triggering the torsional motion has a peak intensity of $1.2 \times 10^{13} \text{ W/cm}^2$ and duration (FWHM) of 1.0 ps. The torsional potential is scaled down by $1/4$ rather than by increasing the kick strength. In practise reduction of the torsional barrier is possible, for instance, by modifying the aromatic rings or by using halogen substituted biphenyl-acetylene.

and the kick pulse needs to be increased either through higher intensity, a longer kick pulse or by trains of synchronized kick pulses [44, 45, 46].

Assuming initial orientation and confinement of the SMPA, we have calculated the ϕ_d dynamics for both conformations the DFDBrBPh molecule with a reduced torsional barrier (see caption to Fig. 9). The results are shown in Fig. 9, and clearly, the present method would allow for a time-resolved study of the transition from one enantiomer into the other. A quantitative analysis of the efficiency of the process shows that after the pulse 99% of the molecules starting out as R_a has changed into S_a enantiomers, whereas only 13% of the S_a enantiomers changed into R_a . The inverse process causing an excess of R_a enantiomers, is achieved simply by inverting the

orientation of the molecules.

We believe that the results presented in this paper also fuel the field of molecular junctions [47, 48, 49] with new possibilities. The conductivity of molecules like biphenyl will depend on the dihedral angle [50], and as such this type of molecules, if placed between two leads, can function as a molecular junction [51, 52, 53, 54] that may be used to control the charge flow and act as, e.g., a switch [43]. Importantly, we can realize quantum control of such a system by means of kick pulse schemes and in this way tailor very specific torsional wave packets [55] to dictate the detailed time-dependent dihedral motion and thereby the current flow through the molecular junction. Seen through the light of controllability, molecular junctions based on laser controlled torsion complements the available schemes, such as the mechanical break junctions [56] and the previously suggested resonantly light driven molecular junctions [57, 58, 59].

VII. CONCLUSION

We presented a fs time-resolved study on laser controlled torsion of axially chiral molecules. Experimentally, the symmetry axis of DFDBrBPh molecules was held fixed in space by a long alignment laser pulse while

a fs kick pulse, polarized perpendicular to the fixed axis, was applied. The torsion as well as the overall rotation of the molecule was monitored with fs time resolution using a delayed probe pulse. To substantiate the observations, we developed an original theoretical model, which produces results in good agreement with the experiment. The model divides the dynamics of the molecule into a the rotation with classical behavior and quantum mechanical torsional dynamics. As such the model provides a transparent physical interpretation of essential features of laser controlled torsion of DFDBrBPh. Based on the theoretical model, we further discussed the extension of the experiment to a setup that will facilitate a fs time-resolved study of de-racemization. Finally, we pointed to perspectives of using molecules like DFDBrBPh in molecular junctions in order to realize laser controlled charge flow.

VIII. ACKNOWLEDGEMENTS

This work was supported by the Carlsberg Foundation, The Lundbeck Foundation, Danish Natural Research Foundation, the Danish Natural Science Research Council, and the Danish Research Agency (Grant no. 217-05-0081).

-
- [1] H. Kallmann and F. Reiche, Z. Phys. **6**, 352 (1921).
 - [2] O. Stern, Z. Phys. A **39**, 751 (1926).
 - [3] S. Y. T. van de Meerakker, H. L. Bethlem, and G. Meijer, Nature Phys. **4**, 595 (2008).
 - [4] H. Stapelfeldt, Hirofumi Sakai, E. Constant, and P. B. Corkum, Phys. Rev. Lett. **79**, 2787 (1997).
 - [5] Hoi Sung Chung, Bum Suk Zhao, Sung Hyup Lee, Sungu Hwang, Keunchang Cho Cho, Sang-Hee Shim, S. Wee Kyung Kang, and Doo Soo Chung, J. Chem. Phys. **114**, 8293 (2001).
 - [6] R. Fulton, A. I. Bishop, M. N. Shneider, and P. F. Barker, Nature Phys. **2**, 465 (2006), ISSN 1745-2473.
 - [7] H. Stapelfeldt and T. Seideman, Rev. Mod. Phys. **75**, 543 (2003).
 - [8] H. Niikura, P. B. Corkum, and D. Villeneuve, Phys. Rev. Lett. **90**, 203601 (2003).
 - [9] B. J. Sussman, D. Townsend, M. Y. Ivanov, and A. Stolow, Science **314**, 278 (2006).
 - [10] B. J. Sussman, M. Y. Ivanov, and A. Stolow, Phys. Rev. A **71**, 051401(R) (2005).
 - [11] E. L. Eliel and A. H. Wilen, *Stereochemistry of Organic Compounds, Chapter 14* (Wiley, New York, 1994).
 - [12] G. Bringmann, A. Mortimer, P. Keller, M. Gresser, J. Garner, and M. Breuning, Angew. Chem. Int. Ed. **44**, 5384 (2005).
 - [13] C. B. Madsen, L. B. Madsen, S. S. Viftrup, M. P. Johansson, T. B. Poulsen, L. Holmegaard, V. Kumarappan, K. A. Jørgensen, and H. Stapelfeldt, Phys. Rev. Lett. **102**, 073007 (2009).
 - [14] F. Grein, J. Phys. Chem. A **106**, 3823 (2002).
 - [15] C. F. Matta, J. Hernández-Trujillo, T.-H. Tang, and R. F. W. Bader, Chem. Eur. J. **9**, 1940 (2003).
 - [16] J. Poater, M. Solà, and F. M. Bickelhaupt, Chem. Eur. J. **12**, 2889 (2006).
 - [17] L. F. Pacios, Struct. Chem. **18**, 785 (2007).
 - [18] B. J. Sussman, J. G. Underwood, R. Lausten, M. Y. Ivanov, and A. Stolow, Phys. Rev. A **73**, 053403 (2006).
 - [19] V. Kumarappan, C. Z. Bisgaard, S. S. Viftrup, L. Holmegaard, and H. Stapelfeldt, J. Chem. Phys. **125**, 194309 (2006).
 - [20] K. Hoki, D. Kröner, and J. Manz, Chem. Phys. **267**, 59 (2001).
 - [21] R. N. Zare, *Angular momentum: understanding spatial aspects in chemistry and physics* (John Wiley, New York, 1988).
 - [22] P. Hohenberg and W. Kohn, Phys. Rev. **136**, B864 (1964).
 - [23] W. Kohn and L. J. Sham, Phys. Rev. **140**, A1133 (1965).
 - [24] A. D. Becke, J. Chem. Phys. **98**, 5648 (1993).
 - [25] C. Lee, W. Yang, and R. G. Parr, Phys. Rev. B **37**, 785 (1988).
 - [26] S. H. Vosko, L. Wilk, and M. Nusair, Can. J. Phys. **58**, 1200 (1980).
 - [27] A. Schäfer, C. Huber, and R. Ahlrichs, J. Chem. Phys. **100**, 5829 (1994).
 - [28] M. P. Johansson and J. Olsen, J. Chem. Theory Comput. **4**, 1460 (2008).
 - [29] R. Ahlrichs, M. Bär, M. Häser, H. Horn, and C. Kölmel, Chem. Phys. Lett. **162**, 165 (1989).
 - [30] P. Deglmann, F. Furche, and R. Ahlrichs, Chem. Phys. Lett. **362**, 511 (2002).
 - [31] N. Miyaura and A. Suzuki, Chem. Rev. **95**, 2457 (1995).

- [32] U. Even, J. Jortner, D. Noy, N. Lavie, and C. Cossart-Magos, *J. Chem. Phys.* **112**, 8068 (2000).
- [33] S. Viftrup, V. Kumarappan, S. Trippel, H. Stapelfeldt, E. Hamilton, and T. Seideman, *Phys. Rev. Lett.* **99**, 143602 (2007).
- [34] K. Faber, *Chem. Eur. J.* **7**, 5004 (2001).
- [35] Y. Fujimura, L. González, K. Hoki, J. Manz, and Y. Ohtsuki, *Chem. Phys. Lett.* **306**, 1 (1999).
- [36] M. Shapiro, E. Frishman, and P. Brumer, *Phys. Rev. Lett.* **84**, 1669 (2000).
- [37] D. Kröner and B. Klaumünzer, *Chem. Phys.* **338**, 268 (2007).
- [38] D. Kröner and B. Klaumünzer, *Phys. Chem. Chem. Phys.* **9**, 5009 (2007).
- [39] B. Friedrich and D. Herschbach, *J. Phys. Chem. A* **103**, 10280 (1999).
- [40] B. Friedrich and D. Herschbach, *J. Chem. Phys.* **111**, 6157 (1999).
- [41] H. Tanji, S. Minemoto, and H. Sakai, *Phys. Rev. A* **72**, 063401 (2005).
- [42] L. Holmegaard, J. H. Nielsen, I. Nevo, H. Stapelfeldt, F. Filsinger, J. Küpper, and G. Meijer, *Phys. Rev. Lett.* **102**, 023001 (2009).
- [43] S. Ramakrishna and T. Seideman, *Phys. Rev. Lett.* **99**, 103001 (2007).
- [44] M. Leibscher, I. Sh. Averbukh, and H. Rabitz, *Phys. Rev. Lett.* **90**, 213001 (2003).
- [45] C. Z. Bisgaard, S. S. Viftrup, and H. Stapelfeldt, *Phys. Rev. A* **73**, 053410 (2006).
- [46] K. F. Lee, I. V. Litvinyuk, P. W. Dooley, M. Spanner, D. M. Villeneuve, and P. B. Corkum, *J. Phys. B* **37**, L43 (2004).
- [47] A. Nitzan and M. A. Ratner, *Science* **300**, 1384 (2003).
- [48] Z. J. Donhauser *et al.*, *Science* **292**, 2303 (2001).
- [49] J. Chen and M. Reed, *Chem. Phys.* **281**, 127 (2002).
- [50] J. M. Seminario, A. G. Zacarias, and J. M. Tour, *J. Am. Chem. Soc.* **120**, 3970 (1998).
- [51] M. Čížek, M. Thoss, and W. Domcke, *Phys. Rev. B* **70**, 125406 (2004).
- [52] M. Čížek, M. Thoss, and W. Domcke, *Czechoslovak Journal of Physics* **55**, 189 (2005).
- [53] C. Benesch, M. Čížek, M. Thoss, and W. Domcke, *Chem. Phys. Lett.* **430**, 355 (2006).
- [54] C. Benesch, M. Čížek, J. Klimeš, I. Kondov, M. Thoss, and W. Domcke, *J. Phys. Chem. C* **112**, 9880 (2008).
- [55] J. Werschnik and E. K. U. Gross, *J. Phys. B* **40**, R175 (2007).
- [56] S. Wu, M. T. González, R. Huber, S. Grunder, M. Mayor, C. Schönenberger, and M. Calame, *Nature Nanotech.* **3**, 569 (2008).
- [57] S. Loudwig and H. Bayley, *J. Am. Chem. Soc.* **128**, 12404 (2006).
- [58] C. Zhang, M.-H. Du, H.-P.-Cheng, X.-G. Zhang, A. E. Roitberg, and J. L. Krause, *Phys. Rev. Lett.* **92**, 158301 (2004).
- [59] M. del Valle, R. Gutiérrez, C. Tejedor, and G. Cuniberti, *Nature Nanotech.* **2**, 176 (2007).